Strength of dry and wet quartz in the low-temperature plasticity regime: insights from nanoindentation

Alberto Ceccato[1], Luca Menegon[2,3], Lars N. Hansen[4,5]

[1] Dipartimento di Scienze Biologiche, Geologiche ed Ambientali – BiGeA, Università di Bologna – Alma Mater Studiorum, via Zamboni, 67, 40126 Bologna – Italy; [2] The Njord Centre, Department of Geosciences, University of Oslo, Postbox 1047 Blindern, 0316 Oslo, Norway; [3] School of Geography, Earth and Environmental Sciences, University of Plymouth, Drake Circus, Plymouth PL48AA, UK; [4] Department of Earth Sciences, University of Oxford, Oxford, UK; [5] Department of Earth and Environmental Sciences, University of Minnesota, Twin Cities, Minneapolis, MN, USA

Corresponding author: Alberto Ceccato (alberto.ceccato@unibo.it.

Key Points

- Occurrence of hydrolytic weakening in quartz in the low-temperature plasticity regime tested by spherical and Berkovich nanoindentation.
- Intracrystalline H_2O content does not affect the strength of quartz in the low-temperature plasticity regime.
- The pre-indentation intracrystalline strain controls the yield strength and hardness of natural quartz.

Abstract.

At low-temperature and high-stress conditions, quartz deformation is controlled by the kinetics of dislocation glide, often referred to as low-temperature plasticity (LTP). To investigate the relationship between intracrystalline H_2O content and the yield strength of quartz during LTP, we have integrated spherical and Berkovich nanoindentation tests at room temperature on natural quartz grains from a deformed migmatitic gneiss with electron backscatter diffraction (EBSD) and secondary-ion mass spectrometry (SIMS) measurements of intracrystalline H_2O content. Dry (<20 wt ppm H_2O) and wet (20–100 wt ppm H_2O) crystals exhibit comparable indentation hardness, which is proportional to quartz yield strength. Thus, quartz yield strength, seems to be unaffected by the intracrystalline H_2O content. Pre-indentation strain history may have had a major role in generating a high density of dislocation sources, which controlled the yield stress during LTP.

Plain Language Summary

Quartz generally contains small amounts of water within its crystal structure. These small amounts may dramatically decrease quartz strength at high temperatures typical of the deeper portions of Earth's crust. At slightly lower temperatures (200–300°C), the effects of these small amount of water on quartz strength is still matter of debate. Here, we present the results of mechanical tests measuring the resistance to the penetration by a microscopic diamond tip of natural quartz grains containing different amounts of water. These experiments are expected to promote the activation of deformation mechanisms experienced by quartz in the intermediate portions of the Earth's crust, where earthquakes commonly nucleate. The results demonstrate that the mechanical resistance of quartz is similar for different intracrystalline water content. Thus, the small amounts of water contained in the quartz crystal structure do not affect its strength. Rather, it seems that the high density of defects in the crystal structure, which developed during the long geological history of natural quartz samples, controls the actual strength of quartz in our experiments, and, by extrapolation, at intermediate depth in Earth's crust.

Keywords

Nanoindentation, Low-temperature plasticity, Quartz, Dislocation glide, Hydrolytic weakening.

1. Introduction

Experimental rock deformation has demonstrated that the strength of quartz is significantly reduced by the presence of intracrystalline H_2O either bonded to the crystal lattice or occurring as micro-fluid inclusions, i.e., quartz exhibits hydrolytic weakening (Ave Lallemant & Carter, 1971; Griggs, 1967; Griggs & Blacic, 1965; Tullis & Yund, 1980). Results from laboratory experiments established that water weakening occurs in both synthetic and natural quartz crystals with intracrystalline H_2O contents larger than 20–30 wt ppm (about 150 H/10^6 Si) (Stünitz et al., 2017 and references therein). Several different microphysical processes have been proposed to explain water weakening in quartz: (1) hydrolyzation of Si-O-Si bonds around dislocations to form weaker Si-OH:HO-Si bonds, consequently decreasing the resistance to dislocation motion (i.e., reducing the Peierls stress) (Griggs, 1967), (2) enhanced dislocation generation around H_2O clusters within the crystal lattice (McLaren et al., 1989; Stünitz et al., 2017), and enhanced recovery through increased ionic diffusivities and faster dislocation climb (Post et al., 1996; Tullis and Yund, 1989).

HyHydrolytic weakening has been experimentally observed in natural and synthetic quartz samples deformed at high homologous temperature, conditions for which dislocation climb and recovery processes are efficient and control the

overall strain rate (Fitz Gerald et al., 2006; Holyoke & Kronenberg, 2013; Kronenberg & Tullis, 1984; Mancktelow & Pennacchioni, 2004; Stipp et al., 2006; Tullis & Yund, 1980). However, there is considerably interest in the deformation of quartz higher stresses and lower temperatures that are characteristic of the strength-controlling portion of the continental crust near the frictional-viscous transition (Goldsby et al., 2004; Lloyd, 2000; Stünitz et al., 2017; Trepmann et al., 2017). At such conditions, often referred to as the low-temperature plasticity (LTP) regime, intracrystalline plasticity of quartz is assumed to be controlled by the kinetics of dislocation glide rather than recovery, and therefore any water weakening is expected to come from either an effective decrease in Peierls stress (Griggs, 1967) or an increase in the dislocation nucleation rate (e.g., Stünitz et al., 2017). However, the possible effect of H_2O, H^+ or OH^- on the resistance to dislocation glide in quartz is still debated (Hartley & Wilshaw, 1973; McLaren et al., 1989; Trepied & Doukhan, 1982). Unfortunately, only very few experiments have been conducted at low temperatures, with conflicting results. For example, based on very few data points, Griggs (1967) argued that hydrolytic weakening occurs in quartz, but only above a threshold temperature of ~400 °C. In contrast, Evans (1984) observed no hydrolytic weakening up to ~900 °C. In addition, both of these previous studies were conducted on synthetic quartz, making extrapolation to geological settings less clear. Thus, an improved understanding of the effect of intracrystalline H_2O on the strength of natural quartz in the LTP regime is essential for future analysis of deformation at high stress in the crust.

Here we address this topic by analysing the hardness of natural quartz grains with different H_2O contents through a series of nanoindentation tests at room conditions (T = 25 °C, P = 1 atm). Nanoindentation is a valuable experimental procedure to investigate dislocation-controlled plasticity at low-temperature conditions, given that the sample surrounding the indented volume experiences large self-confining pressures that suppress brittle deformation (e.g., Evans & Goetze, 1979). Here we implement spherical and Berkovich nanoindentation tests to retrieve the hardness of individual quartz crystals with different amounts of intracrystalline H_2O. Spherical nanoindentation provides an estimate of the yield hardness, which is proportional to the yield stress at which quartz starts to deform plastically by dislocation glide (Pathak & Kalidindi, 2015). The hardness retrieved from Berkovich nanoindentation is considered as a proxy for the post-yield resistance to plastic flow, representing the flow stress at constant indentation strain of 7%. (Fischer-Cripps, 2011). We are primarily interested in the mechanical effects of intracrystalline H_2O on the plastic yield and flow strength of quartz in the LTP regime. Therefore, we are not addressing the mechanisms that may facilitate fluid infiltration and redistribution in quartz (e.g., micro-cracking and crack healing: Stünitz et al., 2017; Trepmann et al., 2017). Nanoindentation has been integrated with measurements of intracrystalline H_2O contents of the indented grains with secondary ion mass spectrometry (SIMS), and with electron backscatter diffraction (EBSD) analysis of the indented grains.

2. Materials and Methods

2.1. Sample material

The two investigated natural quartz aggregates occur in the granulite-facies migmatitic gneisses of the Seiland Igneous Province (northern Norway), which were deformed at T = 760-820 °C and P = 0.75–0.95 GPa (Menegon et al., 2011). Rock chips (1 cm x 1 cm x 0.3 cm) were cut from the leucosome-rich and from the leucosome-poor domain of the migmatitic gneiss sample Ø15 analysed in Menegon et al. (2011). The surface of the rock chip tested with nanoindentation is oriented perpendicular to the foliation and parallel to the stretching lineation (XZ kinematic plane). This surface was prepared for indentation and subsequent electron microscopy by iteratively polishing with diamond suspensions of decreasing grit size, finishing with a grit size of 0.05 m. Quartz grains exhibit internal deformation in both domains, as evidenced by undulatory extinction and the presence of subgrains (Fig. 1a-b). Further details on the initial sample microstructure can be found in Menegon et al. (2011).

2.2. Nanoindentation tests and data analysis

Nanoindentation tests were carried out at the Department of Materials, University of Oxford (UK), using an MTS Nanoindenter XP equipped with Continuous Stiffness Measurement (CSM). Two series of nanoindentation tests were performed at room temperature (25°C) on quartz grains using Berkovich (three-sided pyramid with half angle of 65.27°) and spherical (effective radius of 7 µm) diamond indenter tips. Tests were performed at constant indentation strain rate (defined as loading rate divided by load) of 0.05 s^{-1} up to a maximum depth of 2 µm and a maximum load of 530 mN. Load and displacement into the sample were measured continuously throughout the duration of each test (260 s). Stress-strain curves for spherical nanoindentation tests have been computed from load-displacement data following the approach of Pathak & Kalidindi (2015). The yield hardness has been obtained from graphical evaluation of stress-strain curves. Hardness and elastic modulus were computed from continuous stiffness measurements during Berkovich nanoindentation tests following the approach of Oliver & Pharr (1992). Values of elastic modulus and hardness reported in the text refer to those measured at the maximum load (530 mN). Of the total dataset of nanoindentation tests, only those effectively performed within single, optically-clear grains, away from grain boundaries, fluid inclusion traces, and macroscopic inter-granular fractures (as inferred from EBSD and BSE images), have been considered for further mechanical analysis (136 Berkovich + 68 spherical). Further information about the experimental procedure and processing of mechanical data can be found in the Supplementary material Text S1.

2.3. Secondary ion mass spectrometry (SIMS)

Intracrystalline H_2O content in quartz was measured with the Cameca IMS-4f ion probe at the NERC Ion Microprobe Facility at the University of Edinburgh, UK. Measurements were acquired from the same optically-clear quartz grains on which nanoindentation tests were performed, paying attention to avoid fluid inclusions, cracks, and grain boundaries. The samples were coated with a thin gold film (<0.02 µm) and kept in the SIMS chamber under high vacuum conditions (5 x 10^{-9} Torr) for >48 hours prior to analysis. Analysis was performed with a 5 nA primary beam of $^{16}O^-$ ions accelerated to 14.5 kV. Basaltic glass standard St81A9 (Lesne et al., 2011) was used to calibrate the H_2O contents, whereas an anhydrous olivine standard (Kilbourne Hole) was used to correct for background ^1H signals. H_2O contents calculated as wt ppm H_2O have been converted to $H/10^6$ Si applying the conversion of Gleason and DeSisto (2008) (1 wt ppm H_2O = 6.67 $H/10^6$ Si).

2.4. Electron Backscatter Diffraction (EBSD)

EBSD analysis was performed on selected areas investigated by nanoindentation. Samples have been carbon-coated without any additional (neither mechanical nor chemical) polishing of the surface to preserve residual indentations (Fig. S1). EBSD analysis was performed at the Electron Microscopy Centre of the University of Plymouth (UK) using a JEOL 7001 FEG SEM equipped with a NordLys Max EBSD detector (AZtec acquisition software, Oxford Instruments). EBSD maps were acquired with a step size of 0.3 µm using a 20 kV acceleration voltage, a working distance between 17 and 20 mm, and processed with the AZtec software package (Oxford Instruments). EBSD results are presented as orientation maps and inverse pole figures, in order locate individual indents within the quartz aggregate and to retrieve the crystallographic direction of quartz parallel to the loading direction (Figs. 1c-e; S2). EBSD maps of the grain orientation spread (GOS), grain reference orientation deviation (GROD), and kernel average misorientation (KAM) were derived to evaluate the extent and distribution of intracrystalline deformation and associated substructures near each indent (Figs. 1c-d; S2).

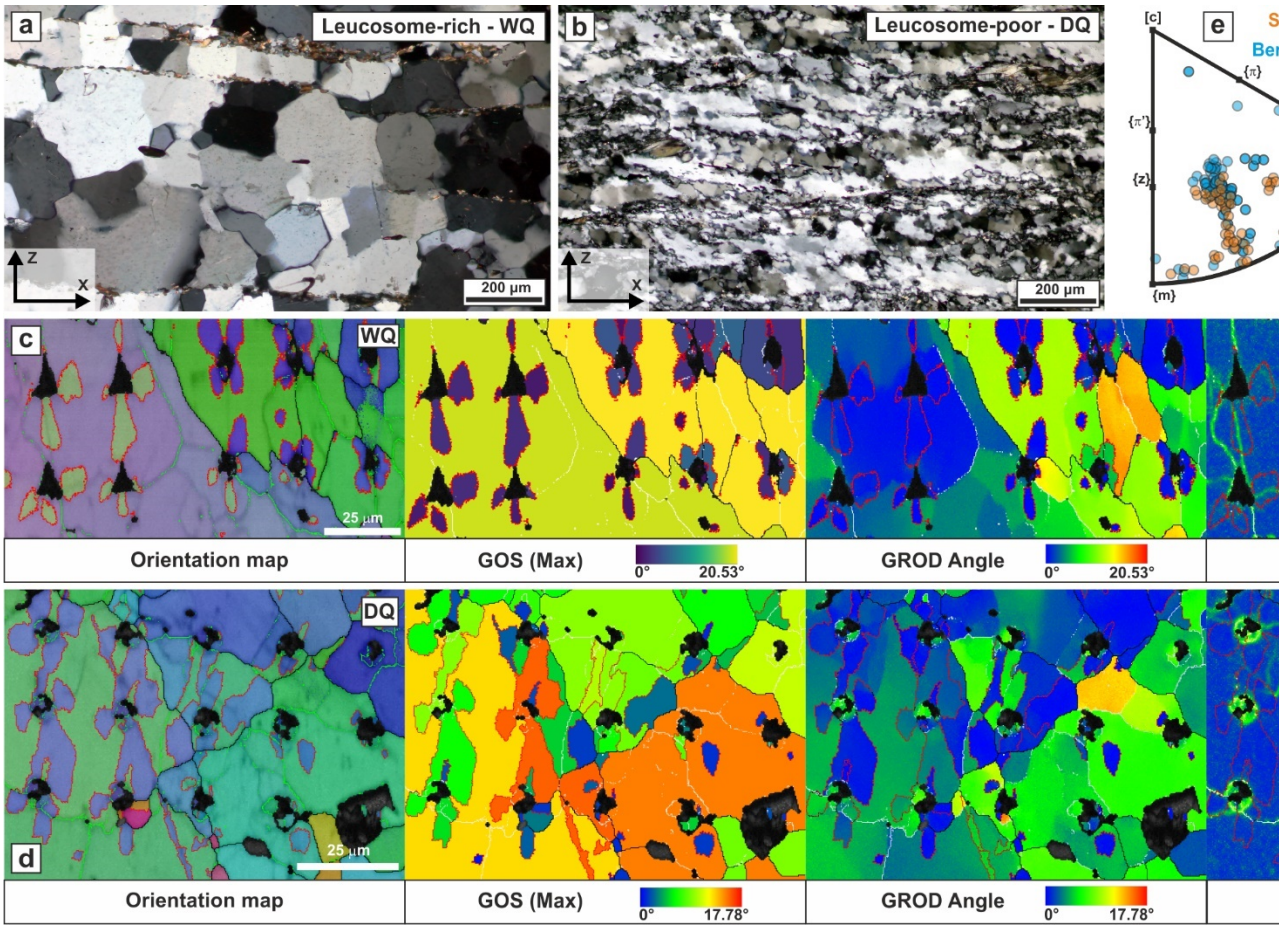

Figure 1

(a and b) Optical microstructure of leucosome-rich and leucosome-poor quartz aggregates adopted for nanoindentation tests (Sample Ø15, Menegon et al., 2011).(c and d) Result of EBSD mapping, for WQ and DQ respectively, including from left to right: orientation map colour coded according to the inverse pole figure for the Y-kinematic direction (colour coded according to the inverse pole figure legend shown in the upper right corner of the figure); maximum grain-orientation spread (GOS) map indicating the maximum value of misorientation from the average orientation of each grain; grain-reference-orientation deviation (GROD) maps indicating the local misorientation of each pixel within a grain with respect to the average grain orientation; and kernel-average misorientation (KAM) maps indicating the local misorientation (up to 4°) at each pixel based on a 5x5 grid of neighbouring pixels. (e) Inverse pole figure indicating the crystallographic directions of quartz crystals parallel to the indentation direction

(Y) for Berkovich (light blue dots) and spherical (orange dots) nanoindentation as inferred from EBSD orientation maps.

3. Results

3.1 SIMS – H_2O-content analysis

SIMS analyses from quartz in leucosome-poor samples reveal H_2O contents ranging between 15 and 27 wt ppm of H_2O (average of 18 ppm over 5 measurements). Quartz in leucosome-rich samples reveal H_2O contents ranging between 2 ppm and 104 ppm (average of 45 ppm over 13 measurements). SIMS results are in agreement with the values obtained by Menegon et al (2011) by FTIR analysis of the Ø15 sample. Given the observed scatter in the measured H_2O contents, SIMS data and the related results of nanoindentation tests and EBSD analyses have been divided into two datasets ("dry quartz" – DQ; "wet quartz" – WQ; Fig. 2) considering 20 wt ppm H_2O as the threshold above which quartz grains are commonly considered "wet" (Milke et al., 2013; Stünitz et al., 2017). Quartz grains with <20 wt ppm H_2O have been assigned to the "dry quartz" (DQ) dataset (2-18 wt ppm H_2O over 7 measurements; Fig. 2), whereas quartz grains with >20 wt ppm H_2O to the "wet quartz" (WQ) dataset (27-104 wt ppm H_2O over 11 measurements; Fig. 2), regardless of the location of the grain (leucosome-rich vs leucosome-poor domain).

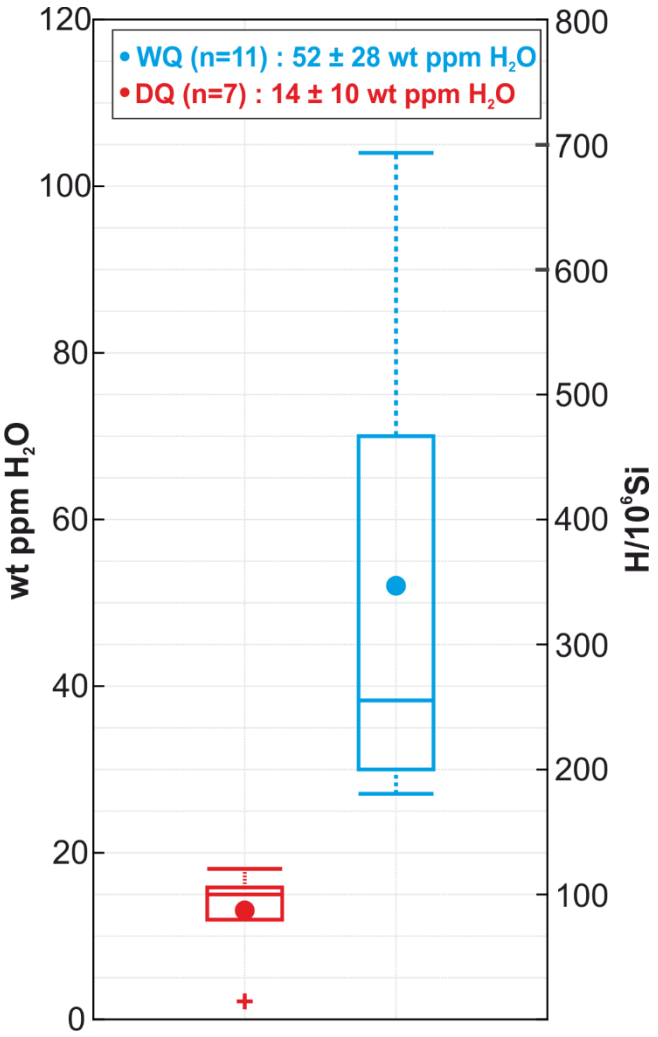

Figure 2

Box-and-whisker plot presenting the H_2O content of DQ and WQ samples as obtained from SIMS analysis. The inset reports the mean and 2 values of measured wt ppm H_2O.

3.2 EBSD maps

Nanoindentation tests were performed mainly either parallel to directions halfway between <r> and <z> or normal to [c] crystal directions (Fig. 1e) as a consequence of the strong crystallographic preferred orientation of both natural quartz samples (Menegon et al., 2011). Dauphiné twins are widespread

around indents forming four-fold lobes (Fig. 1c-d), as similarly observed by previous studies (Ferguson et al., 1987; Hartley & Wilshaw, 1973; Lloyd, 2000).

The indented grains in both DQ and WQ have maximum grain orientation spread generally >8° (GOS in Fig. 1c-d). The EBSD maps highlight the presence of (i) internal bands with misorientation of up to 21° with respect to the average orientation of the grain (GROD in Fig. 1c-d) and (ii) a high density of low-angle boundaries surrounding regions of low local misorientation (KAM in Figs. 1c-d). Additional EBSD maps and SE images of indents can be found in the Supplement (Fig. S1-S2).

3.3 Nanoindentation tests

3.3.1. Spherical nanoindentation tests

Load-displacement curves for spherical nanoindentation tests exhibit (Fig. 3a-b) (i) residual displacements, indicating plastic deformation, and (ii) rare "steps" in the loading portion of the load-displacement curve, usually referred to as "pop-ins" (hollow circles in Fig. 3a-b). We note that these pop-ins are considerably smaller than what is commonly reported in literature (e.g., Kumamoto et al., 2017; Pathak & Kalidindi, 2015). The yield hardness is usually retrieved from graphic evaluation of stress-strain curves as the breakpoint in the slope between the first segment of the curve, exhibiting a linear relationship between stress and strain, and the remaining part of the curve showing a generally less steep slope describing the plastic behaviour of the sample (Kumamoto et al., 2017; Pathak & Kalidindi, 2015). However, there can be ambiguity in stress-strain curves, and in many of our tests it is possible to define two breakpoints (Fig. 3c-d). For each indent, we report the stress values of both points along the stress-strain curve as Yp_1 and Yp_2. At stresses above both Yp_1 and Yp_2, the stress conditions continue to increase with strain, which is consistent with the strain hardening previously observed in nanoindentation tests on other geological materials in the LTP regime (Kranjc et al., 2016; Kumamoto et al., 2017). The corresponding values of hardness at Yp_1 and Yp_2 are reported in Fig. 4a for the whole dataset. Both Yp_1 and Yp_2 yield points occur over a wide range of stress conditions, yet comparable for both WQ and DQ samples (Fig. 4a). The hardness at Yp_1 for WQ (5.8 ± 2 GPa [2]) is statistically indistinguishable from the value at Yp_1 for DQ (6.1 ± 2 GPa). Similarly, hardness at Yp_2 for WQ (10.9 ± 3 GPa) is also statistically indistinguishable from the value at Yp_2 for DQ (11.7 ± 2 GPa). Some of the variability in yield hardnesses can be attributed to plastic anisotropy, as best evidenced by Yp_1 in WQ, for which values of Yp_1 derived from tests performed parallel to <a> and <m> (6.0–8.5 GPa) are on average larger than those obtained from indentation parallel to crystal directions intermediate to <r> and <z> (<6.0 GPa; Fig. 4b).

3.3.2. Berkovich nanoindentation tests

Load-displacement curves from Berkovich nanoindentation tests exhibit a residual displacement of ~0.8 µm (Fig. 3e-f). Elastic moduli calculated at maximum load (530 mN) for WQ and DQ range between 84 and 107 GPa (98.7 ± 12 GPa), and 79 and 107 GPa (92.1 ± 11 GPa), respectively (Fig. 4d). Elastic moduli are comparable (within 5–10%) with the elastic modulus predicted for right-handed -quartz (Ogi et al., 2006), with larger values for quartz samples indented parallel to <r-z> than those obtained from samples indented parallel to <a-m> (Fig. 4e). Hardness values for WQ and DQ at maximum load conditions ranges between 9 and 13.5 GPa (11.7 ± 2 GPa), and 8 and 13 GPa (10.6 ± 2 GPa), respectively (Fig. 4d). DQ samples indented parallel to <a> and <m> directions exhibit significantly (up to 4 GPa) lower hardness values compared to WQ samples indented close to <r-z> (Fig. 4f). During sample loading, hardness decreases with increasing indentation depth into the sample (Supplement S3).

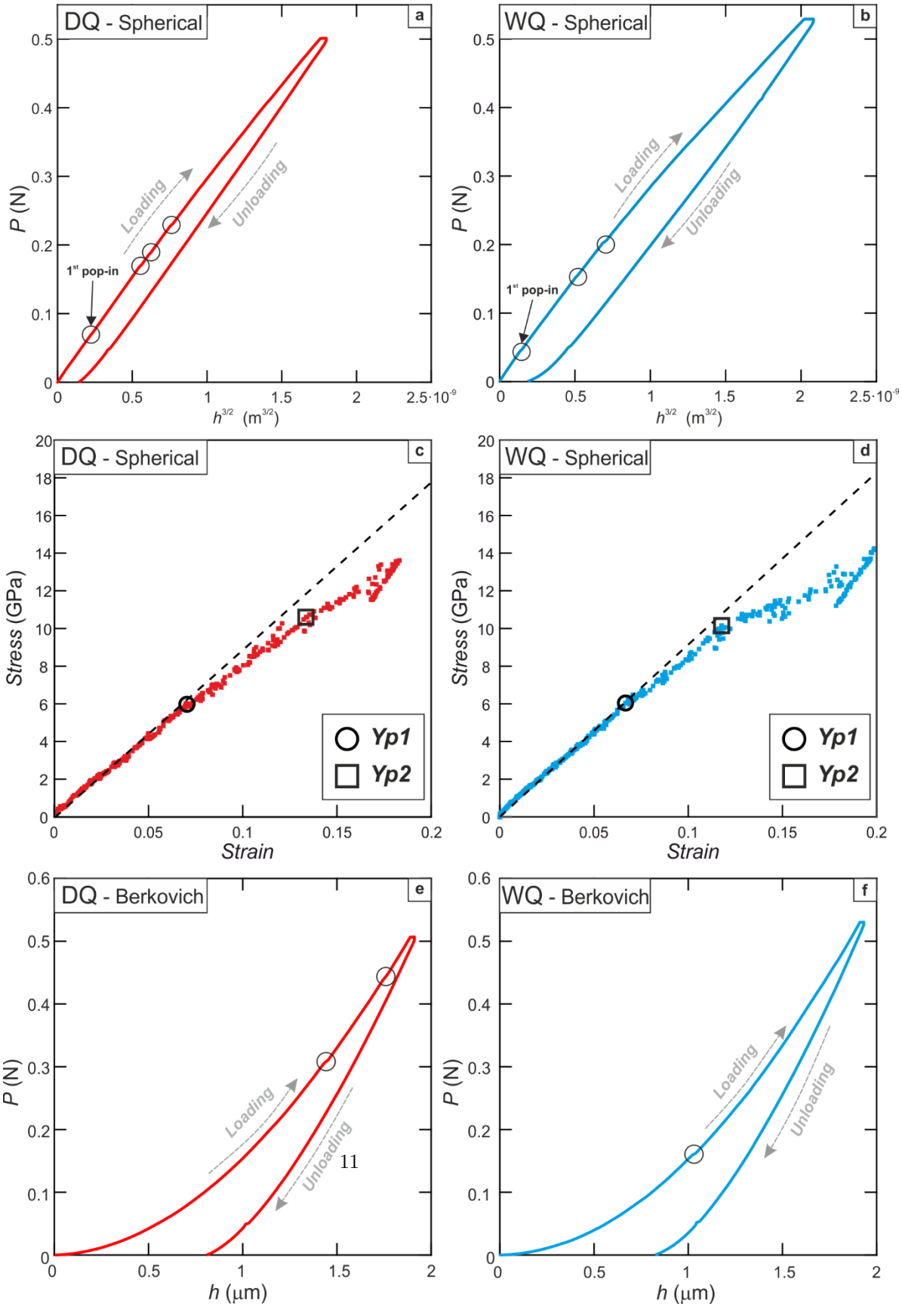
DQ - Spherical
a
P (N)
h^3/2 (m^3/2)
1st pop-in
Loading
Unloading
WQ - Spherical
b
DQ - Spherical
c
Stress (GPa)
Strain
Yp1
Yp2
WQ - Spherical
d
DQ - Berkovich
e
h (μm)
WQ - Berkovich
f

Figure 3

Load-displacement and stress-strain diagrams resulting from spherical and Berkovich nanoindentation tests. (a and b) Load-displacement diagrams of representative spherical nanoindentation tests for DQ and WQ samples, respectively. Purely elastic behaviour of the sample would be represented by a linear relationship between $(\text{Displacement})^{3/2}$ and Load. Circled points along load-displacement curves represent the occurrence of a pop-in during loading. (c and d) Stress-strain curves calculated from spherical nanoindentation for DQ and WQ respectively. Both curves present two breakpoints (Yp_1 and Yp_2) at which the slope changes, and either could be taken to represent the yield conditions [see text for explanation]. (d and e) Load-displacement diagram of representative Berkovich nanoindentation tests for DQ and WQ samples, respectively.

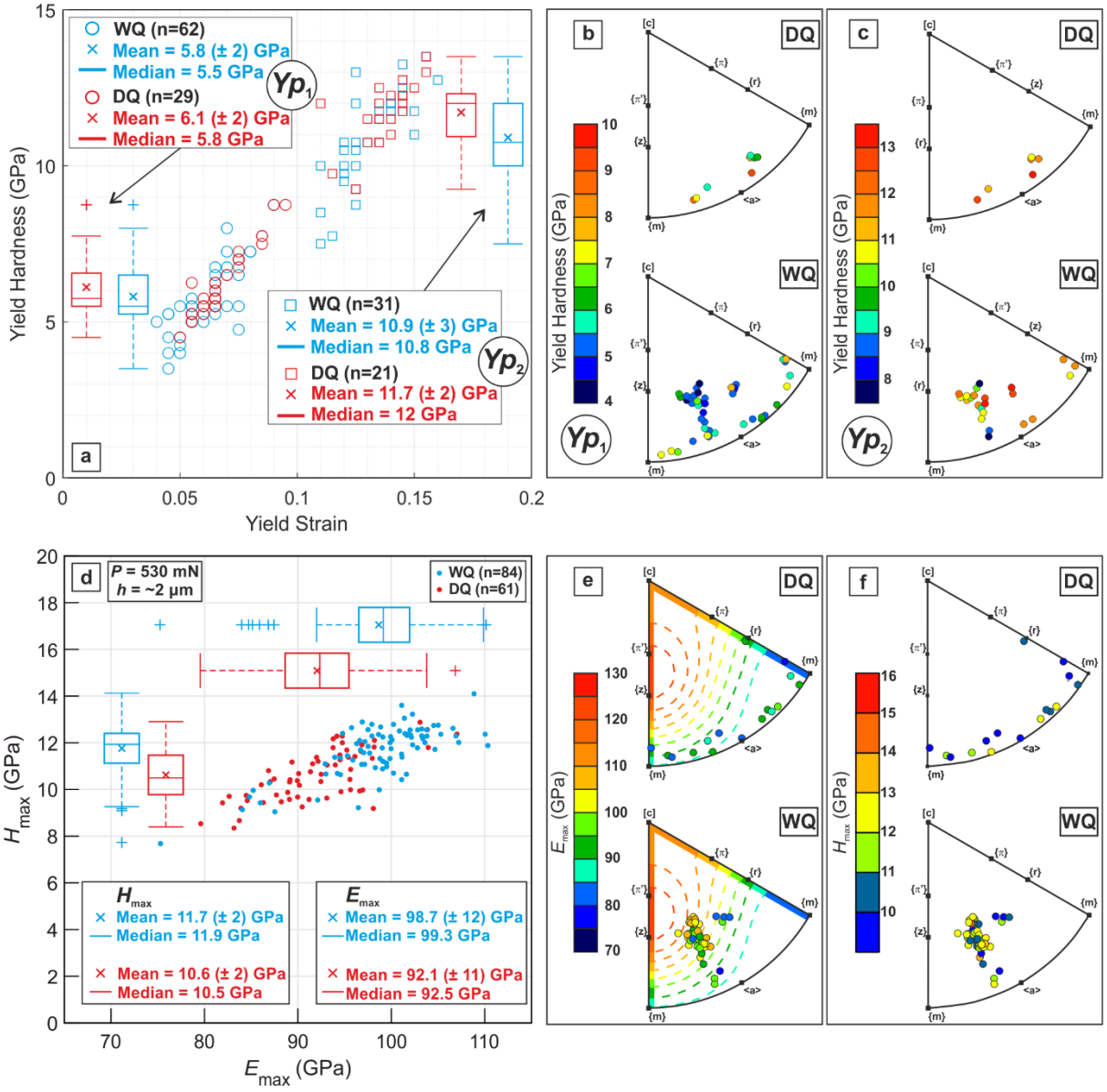

Figure 4

Results of hardness measurements from nanoindentation tests. (a) Stress-strain scatter diagram and box-and-whiskers plot indicating the distribution of yield hardness-strain conditions for the identified breakpoints Yp_1 and Yp_2 along stress-strain curves. The insets report the mean, median, and 2 (in bracket) of the yield hardness of each dataset. (b) Inverse pole figures for quartz illus-

trate the yield hardness values for Yp_1 and Yp_2 for each tested crystallographic direction in DQ and WQ samples. (d) Hardness vs. elastic modulus scatter plot indicating the distribution of $H_{\max}$-$E_{\max}$ values obtained from Berkovich nanoindentation on WQ and DQ samples. The insets report the mean, median, and 2 (in bracket) of the elastic modulus and hardness of each dataset. (e) Inverse pole figures for quartz illustrating the elastic modulus values for each tested crystallographic direction. The dashed contour lines represent the expected variation of elastic modulus as calculated from the elastic tensor of dry and wet quartz at room temperature (Ogi et al., 2006). (f) Inverse pole figures for quartz illustrating the indentation hardness values for each tested crystallographic direction.

4. Discussion and Conclusion

The range of intracrystalline H_2O content in DQ and WQ is relatively narrow, but it encompasses the transition from what is normally considered "dry" and "wet" quartz in deformation experiments, at around 20–30 wt ppm H_2O (Stünitz et al., 2017). At low-temperature conditions, hydrolytic weakening is expected to either increase the dislocation density by promoting dislocation nucleation and multiplication around intracrystalline H_2O defects (McLaren et al., 1989; Stünitz et al., 2017), or decreasing the Peierls stress by covalent bond hydrolyzation around dislocations (Griggs, 1967).

The experiments presented here allow us to test these expectations by conducting identical experiments on the two groups of quartz grains. The results of indentation experiments are notoriously difficult to compare directly to other types of mechanical effects because of the complicated deformation geometry and potential effects related to the scale of deformation (Kumamoto et al., 2017). For instance, the hardness in our Berkovich tests decreases with indentation depth, indicating the occurrence of a "size-effect" in quartz (Fig. S3). However, our analysis of hardness values from the same Berkovich indentation depth or the yield hardness obtained with the spherical indenter of the same radius allows direct comparison within our data set.

Our comparison of indents conduct on wet and dry grains of quartz demonstrates that:

1. For the range of intracrystalline H_2O content sampled here, both the spherical yield hardness and Berkovich hardness do not systematically differ between WQ and DQ grains. These observations suggests that neither the yield stress (and by proxy the Peierls stress) nor the flow strength of quartz are affected by the intracrystalline H_2O content. Thus, the apparent lack of a reduction in Peierls stress suggests hydrolytic weakening by covalent bond hydrolyzation is not efficient in the LTP regime. We note that our results cannot rule out a reduction of the Peierls stress at intermediate temperatures as suggested by Griggs (1967).

2. Load-displacement curves are characterised by rare, low-intensity pop-ins. The lack of more substantial pop-ins suggests a high density of dislocation sources is available (Kumamoto et al., 2017) within both WQ and DQ grains. This observation suggests that the different intracrystalline H_2O content of WQ and DQ did not influenced the nucleation and multiplication of dislocations (c.f. McLaren et al., 1989; Stünitz et al., 2017).

3. WQ and DQ grains are characterised by significant lattice curvature, localized misorientation bands, and high densities of low-angle boundaries (Fig. 1c-d), resulting from the geological, pre-indentation crystal-plastic deformation history (Menegon et al., 2011). These substructures are indicative of an inherited high dislocation density of the natural samples and have likely acted as the dominant dislocation sources during nanoindentation (e.g., Pathak & Kalidindi, 2015), dominating over any possible influence of intracrystalline H_2O on dislocation nucleation and multiplication. Thus, the pre-indentation strain history of quartz in the Ø15 sample might have masked the potential effect of intracrystalline H_2O content on plastic yield strength, by generating a consistently high density of dislocation sources in all the tested grains.

These results provide critical insight into the strength of quartz-rich shear zones in the continental crust during their exhumation approaching the frictional-viscous transition (e.g., Giuntoli et al., 2020; Handy et al., 2007). Under such conditions, progressively lower temperatures and increasing stresses promote LTP and hinder recovery processes (Trepmann et al., 2017; Trepmann & Seybold, 2019). Our results indicate that the kinetics of dislocation glide in the LTP regime will not be affected by the intracrystalline H_2O content of quartz, as it is otherwise expected for dislocation creep-controlled deformation at higher-temperature (Kilian et al., 2016; Palazzin et al., 2018). Furthermore, the intracrystalline strain history inherited from higher-temperature deformation at deeper crustal conditions may play a more important role than intracrystalline H_2O content in controlling the yield strength of quartz. Yet, other mechanisms (e.g., dislocation multiplication related to micro-fluid inclusions) or intracrystalline H_2O contents larger than those sampled here (i.e., »100 wt ppm H_2O), might be necessary to promote hydrolytic weakening during LTP in natural samples with an inherited intracrystalline strain (Stünitz et al., 2017). We cannot exclude that hydrolytic weakening may still occur during LTP in strain-free, H_2O-rich quartz crystals, for example in quartz grains in synkinematic veins, which frequently localize strain at the base of the seismogenic zone in the middle crust (Ceccato et al., 2017; Handy et al., 2007; Marchesini et al., 2019; Pennacchioni et al., 2010). Further nanoindentation experiments on selected vein quartz grains are required to test this hypothesis.

Acknowledgments, Samples, and Data.

This study was supported by the FP7 Marie Curie CIG "EVOCOS" to LM. Cees-Jan De Hoog and the staff at the NERC Ion Microprobe Facility in Edinburgh are thanked for their support during SIMS analysis. The Authors declare they have no perceived financial conflicts of interests with respect to the results of this paper.

Open Research – Data availability statement

Datasets for this research are available at http://dx.doi.org/10.17632/56sgvzvhvc.2 (Ceccato, Alberto; Menegon, Luca; Hansen, Lars Norman (2021), "Nanoindentation-SIMS_datasets_GRL", Mendeley Data, V2).

References

Ave Lallemant, H. G., & Carter, N. L. (1971). Pressure dependence of quartz deformation lamellae orientations. *American Journal of Science*. https://doi.org/10.2475/ajs.270.3.218

Ceccato, A., Pennacchioni, G., Menegon, L., & Bestmann, M. (2017). Crystallographic control and texture inheritance during mylonitization of coarse grained quartz veins. *Lithos*, *290–291*. https://doi.org/10.1016/j.lithos.2017.08.005

Evans, B. (1984). The effect of temperature and impurity content on indentation hardness of quartz. *Journal of Geophysical Research: Solid Earth*, 89(B6), 4213–4222.

Evans, B., & Goetze, C. (1979). The temperature variation of hardness of Olivine and its implications for polycrystalline yield stress. *Journal of Geophisical Research: Solid Earth*, *84*(8).

Ferguson, C. C., Lloyd, G. E., & Knipe, R. J. (1987). Fracture mechanics and deformation processes in natural quartz : a combined Vickers identification, SEM, and TEM study. *Canadian Journal of Earth Sciences*, *24*(3), 544–555. https://doi.org/10.1139/e87-053

Fischer-Cripps, A. C. (2011). *Nanoindentation. Mechanical Engineering Series - Springer*. https://doi.org/10.1057/9781137525833.0001

Fitz Gerald, J. D., Mancktelow, N. S., Pennacchioni, G., & Kunze, K. (2006). Ultrafine-grained quartz mylonites from high-grade shear zones: Evidence for strong dry middle to lower crust. *Geology*. https://doi.org/10.1130/G22099.1

Giuntoli, F., Menegon, L., Warren, C. J., Darling, J., & Anderson, M. W. (2020). Protracted Shearing at Midcrustal Conditions During Large-Scale Thrusting in the Scandinavian Caledonides. *Tectonics*, *39*(9), 1–31. https://doi.org/10.1029/2020TC006267

Gleason, G. C., & DeSisto, S. (2008). A natural example of crystal-plastic deformation enhancing the incorporation of water into quartz. *Tectonophysics*, 446(1–4), 16–30. https://doi.org/10.1016/j.tecto.2007.09.006

Goldsby, D. L., Rar, A., Pharr, G. M., & Tullis, T. E. (2004). Nanoindentation creep of quartz, with implications for rate- and state-variable friction laws relevant to earthquake mechanics. *Journal of Materials Research*, *19*(1), 357–365. https://doi.org/10.1557/jmr.2004.19.1.357

Griggs, D. T. (1967). Hydrolytic Weakening of Quartz and Other Silicates. *Geophysical Journal of the Royal Astronomical Society*. https://doi.org/10.1111/j.1365-246X.1967.tb06218.x

Griggs, D. T., & Blacic, J. D. (1965). Quartz: Anomalous weakness of synthetic crystals. *Science*. https://doi.org/10.1126/science.147.3655.292

Handy, M. R., Hirth, G., & Bürgmann, R. (2007). Continental Fault Structure and Rheology from the Frictional-to-Viscous Transition Downward. In *Tectonic Faults* (pp. 139–181). https://doi.org/10.7551/mitpress/6703.003.0008

Hartley, N. E. W., & Wilshaw, T. R. (1973). Deformation and fracture of synthetic -quartz. *Journal of Materials Science*, *8*(2), 265–278. https://doi.org/10.1007/BF00550676

Holyoke, C. W., & Kronenberg, A. K. (2013). Reversible water weakening of quartz. *Earth and Planetary Science Letters*. https://doi.org/10.1016/j.epsl.2013.05.039

Kilian, R., Heilbronner, R., Holyoke, C. W., Kronenberg, A. K., & Stünitz, H. (2016). Dislocation creep of dry quartz. *Journal of Geophysical Research: Solid Earth*. https://doi.org/10.1002/2015JB012771

Kranjc, K., Rouse, Z., Flores, K. M., & Skemer, P. (2016). Low-temperature plastic rheology of olivine determined by nanoindentation, *43*, 176–184. https://doi.org/10.1002/2015GL065837.Received

Kronenberg, A. K., & Tullis, J. (1984). Flow strength of quartz aggregates: grain size and pressure effects due to hydrolytic weakening. *Journal of Geophysical Research*, *89*(B6), 4281–4297. https://doi.org/10.1029/jb089ib06p04281

Kumamoto, K. M., Thom, C. A., Wallis, D., Hansen, L. N., Armstrong, D. E. J., Warren, J. M., et al. (2017). Size effects resolve discrepancies in 40 years of work on low-temperature plasticity in olivine. *Science Advances*, *3*(9), 1–7. https://doi.org/10.1126/sciadv.1701338

Lesne, P., Scaillet, B., Pichavant, M., Iacono-Marziano, G., & Beny, J. M. (2011). The H2O solubility of alkali basaltic melts: An experimental study. *Contributions to Mineralogy and Petrology*, *162*(1), 133–151. https://doi.org/10.1007/s00410-010-0588-x

Lloyd, G. E. (2000). Grain boundary contact effects during faulting of quartzite: An SEM/EBSD analysis. *Journal of Structural Geology*, *22*(11–12), 1675–1693. https://doi.org/10.1016/S0191-8141(00)00069-9

Mancktelow, N. S., & Pennacchioni, G. (2004). The influence of grain boundary fluids on the microstructure of quartz-feldspar mylonites. *Journal of Structural Geology*. https://doi.org/10.1016/S0191-8141(03)00081-6

Marchesini, B., Garofalo, P. S., Menegon, L., Mattila, J., & Viola, G. (2019). Fluid-mediated, brittle-ductile deformation at seismogenic depth - Part 1: Fluid record and deformation history of fault veins in a nuclear waste repository (Olkiluoto Island, Finland). *Solid Earth*, *10*(3), 809–838. https://doi.org/10.5194/se-10-809-2019

McLaren, A. C., Fitz Gerald, J. D., & Gerretsen, J. (1989). Dislocation nucleation and multiplication in synthetic quartz: Relevance to water weakening. *Physics and Chemistry of Minerals*, *16*(5), 465–482. https://doi.org/10.1007/BF00197016

Menegon, L., Nasipuri, P., Stünitz, H., Behrens, H., & Ravna, E. (2011). Dry and strong quartz during deformation of the lower crust in the presence of melt. *Journal of Geophysical Research: Solid Earth*, *116*(10), 1–23. https://doi.org/10.1029/2011JB008371

Milke, R., Neusser, G., Kolzer, K., & Wunder, B. (2013). Very little water is necessary to make a dry solid silicate system wet. *Geology*. https://doi.org/10.1130/G33674.1

Ogi, H., Ohmori, T., Nakamura, N., & Hirao, M. (2006). Elastic, anelastic, and piezoelectric coefficients of -quartz determined by resonance ultrasound spectroscopy. *Journal of Applied Physics*. https://doi.org/10.1063/1.2335684

Oliver, W. C., & Pharr, G. M. (1992). An improved technique for determining hardness and elastic modulus using load and displacement sensing indentation experiments. *Journal of Materials Research*. https://doi.org/10.1557/JMR.1992.1564

Palazzin, G., Raimbourg, H., Stünitz, H., Heilbronner, R., Neufeld, K., & Précigout, J. (2018). Evolution in H2O contents during deformation of polycrystalline quartz: An experimental study. *Journal of Structural Geology*, *114*, 95–110. https://doi.org/10.1016/j.jsg.2018.05.021

Pathak, S., & Kalidindi, S. R. (2015). Spherical nanoindentation stress-strain curves. *Materials Science and Engineering R: Reports*, *91*, 1–36. https://doi.org/10.1016/j.mser.2015.02.001

Pennacchioni, G., Menegon, L., Leiss, B., Nestola, F., & Bromiley, G. (2010). Development of crystallographic preferred orientation and microstructure during plastic deformation of natural coarse-grained quartz veins. *Journal of Geophysical Research: Solid Earth*. https://doi.org/10.1029/2010JB007674

Post, A. D., Tullis, J., & Yund, R. A. (1996). Effects of chemical environment on dislocation creep of quartzite. *Journal of Geophysical Research: Solid Earth*, 101(B10), 22143–22155. https://doi.org/10.1029/96jb01926

Stipp, M., Tullis, J., & Behrens, H. (2006). Effect of water on the dislocation creep microstructure and flow stress of quartz and implications for the recrystallized grain size piezometer. *Journal of Geophysical Research: Solid Earth*. https://doi.org/10.1029/2005JB003852

Stünitz, H., Thust, A., Heilbronner, R., Behrens, H., Kilian, R., Tarantola, A., & Fitz Gerald, J. D. (2017). Water redistribution in experimentally deformed natural milky quartz single crystals—Implications for H 2 O-weakening processes. *Journal of Geophysical Research: Solid Earth*, *122*(2), 866–894. https://doi.org/10.1002/2016JB013533

Trepied, L., & Doukhan, J. C. (1982). Transmission Electron Microscopy Study of Quartz Single Crystals Deformed At Room Temperature and Atmospheric Pressure By Indentations. *Journal de Physique. Lettres*, *43*(3), 77–81. https://doi.org/10.1051/jphyslet:0198200430307700

Trepmann, C. A., & Seybold, L. (2019). Deformation at low and high stress-loading rates. *Geoscience Frontiers*. https://doi.org/10.1016/j.gsf.2018.05.002

Trepmann, C. A., Hsu, C., Hentschel, F., Döhler, K., Schneider, C., & Wichmann, V. (2017). Recrystallization of quartz after low-temperature plasticity – The record of stress relaxation below the seismogenic zone. *Journal of Structural Geology*. https://doi.org/10.1016/j.jsg.2016.12.004

Tullis, J., & Yund, R. A. (1980). Hydrolytic weakening of experimentally deformed Westerly granite and Hale albite rock. *Journal of Structural Geology*. https://doi.org/10.1016/0191-8141(80)90005-X

Tullis, J., & Yund, R. A. (1989). Hydrolytic weakening of quartz aggregates: The effects of water and pressure on recovery. *Geophysical Research Letters*, 16(11), 1343–1346. https://doi.org/10.1029/GL016i011p01343